Deep Mining 2024 – P Andrieux & D Cumming-Potvin (eds)

doi:10.36487/ACG_repo/2465_90

A modelling approach for underground mine-scale analysis

Xin Wang [a,b,*], Ziqiang Zeng [a,b], Ankang Xing [a,b], Guangliang Yan [c], Xiaonan Wang [c]

[a] *Key Laboratory of Ministry of Education on Safe Mining of Deep Metal Mines, Northeastern University, China*

[b] *Institute of Deep Engineering and Intelligent Technology, Northeastern University, China*

[c] *Benxi Longxin Mining Co., Ltd, China*

Abstract

Deep and high stress underground mining normally has to address the challenges of mining safety and maintaining production capacity. Sishanling iron ore mine, located in Benxi, China, has an extra-thick (247 m) and large sized ore deposit. The first mining stope is located 1.2 km below the surface. To meet the production requirement, the stope is designed with dimensions of 20 m (width), 40 m (length) and 60 m (height), using a deep hole delayed backfilling method. Given the high ground stress conditions, stress management is essential for safe and efficient production from a strategic standpoint. Deep understanding of geological information and a proper mining sequence design are essential in terms of stress management. In this study, a 3D geological model was built using implicit modelling, using drillhole data as the primary geological information. The key components of the 3D geological model include data preprocessing, geological interfaces and block models. Moreover, a campaign of mechanical parameters for the core samples from drillholes was conducted, and the measured data was then interpolated and assigned into the block units within the geological model. Based on the actual scanned geometry data of ramp, drift, crosscut and, most importantly, the designed stope geometry, a mine-scale numerical model was built using FLAC3D to investigate the stability of stopes at mining levels. A numerical method considering development mining backfilling was proposed for underground metal mines. The stress evolution was studied for a simplified mining stope sequence, and the high-risk areas were investigated in terms of stress concentration at the mining front and the volume of the yield rock masses. The proposed comprehensive geological model and full-mine case modelling can provide a practical tool for the analysis and design of the optimal mining sequence.

Keywords: *deep mining, ground stress control, 3D geological modelling, mine-wide numerical modelling*

1 Introduction

Sishanling iron ore mine (Figure 1), owned and operated by Benxi Longxin Mining Co., Ltd., is one of the largest single iron ore deposits in China, with ore reserves estimated at 2.49 billion tonnes. The mining depth is around 1,200 m and its design production capacity is 15 million tonnes per year. The dimensions of the panel area are 500 m length, 200 m width and 60 m height. To meet production demands, stopes are designed with the dimensions of 20 m width, 40 m length and 60 m height, and the deep hole delayed backfilling mining method is employed. Deep underground mining under high stress conditions typically encounters challenges related to mining safety and maintaining production capacity. An effective management of mining-induced stress is essential to ensure a safe and high-capacity production when deep mining. Traditional design concepts that focus on localised structural strength are usually ineffective in considering the whole mining scale picture. Implementing a global approach to stress management is imperative to disperse stress and prevent stress concentrations in the surrounding rock mass, thereby mitigating potential threats to mining safety. Accurate mine geological knowledge forms the basis of various engineering considerations (i.e., Yu et al. 2023; Wang et al. 2021), including mine design, stress control and disaster prevention. A reasonable mine-scale model is crucial

* Corresponding author. Email address: wangx@mail.neu.edu.cn

for a large-scale, concentrated orebodies mining plan, and is especially significant for mining-induced stress management. In this study, a 3D geological modelling approach is developed based on the field drilling data and the geological model is then transferred to FLAC3D models with certain important rock mass properties. Finally, a simplified mining sequence is modelled which considers the stope excavation and backfilling process to demonstrate the proposed approach.

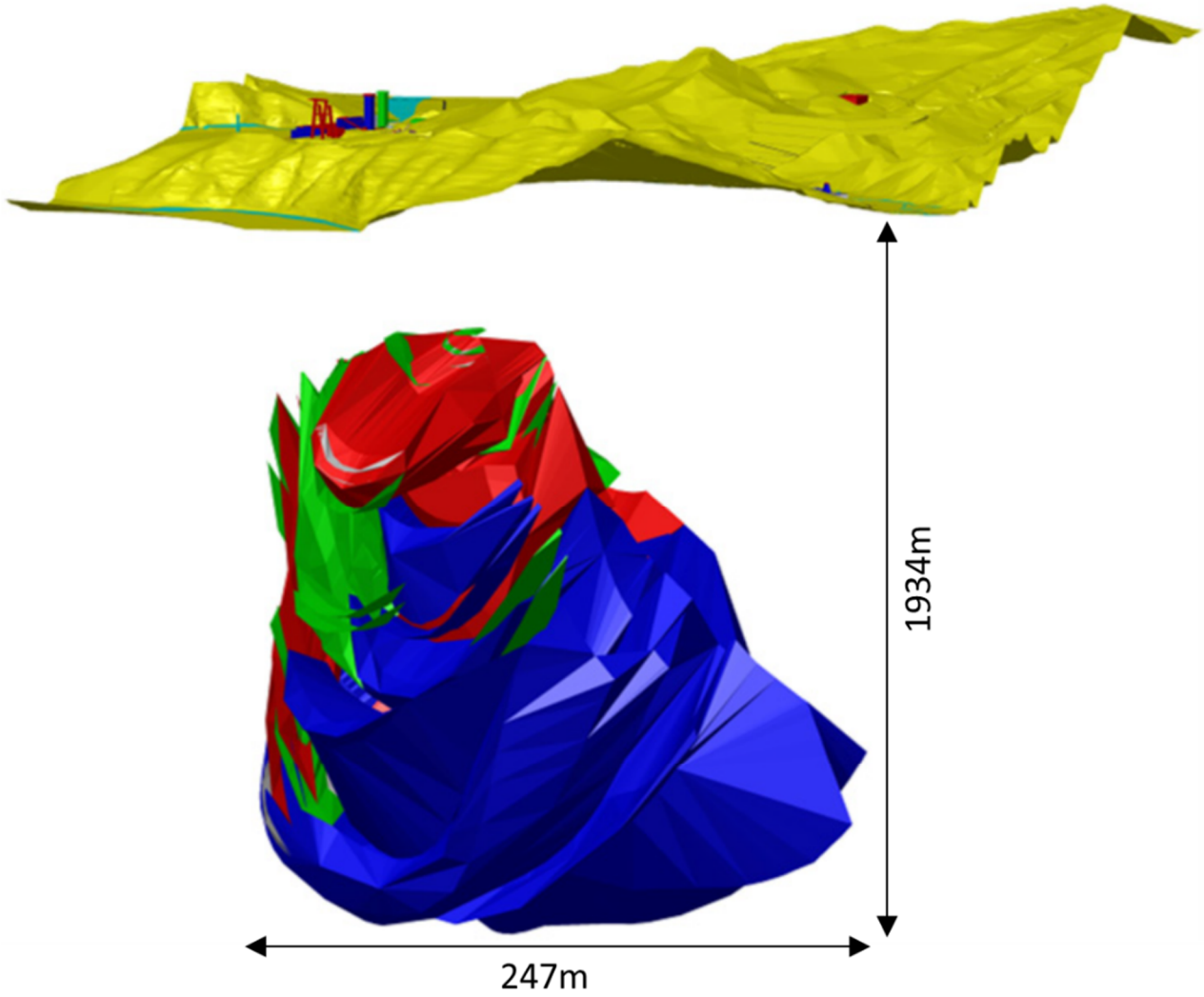

Figure 1 Shape and size of the Sishanling iron orebody

2 3D geological modelling

2.1 Modelling database

A solid database is the foundation for a useful and reliable model (i.e. Kaufmann et al. 2009; Zhong et al. 2019). This study gathers a variety of data within the study area of the Sishanling iron ore mine, such as topographic and geological maps, exploration line profiles and, of course, exploration drilling data (Table 1 and Figure 2). The drilling database comprises a total of 53 drillholes with a total length of 70,841.87 m, and the average length is approximately 1,300 m. The length of the ore sample is 21,830.90 m, which accounting for 30.82% of the total length of the drillholes. The lithologies, from surface to the deep, are marl, quartz sandstone, quartzite, phyllite, dolomitic marble, ore, hematite quartzite, chlorite schist and migmatitic granite (see Figure 2). This database will support the next step of 3D geological modelling of the Sishanling iron ore mine. The modelling data sources primarily include regional satellite maps, topographic and geological maps, exploration line profiles, drillhole data and preliminary design documents for the mining project.

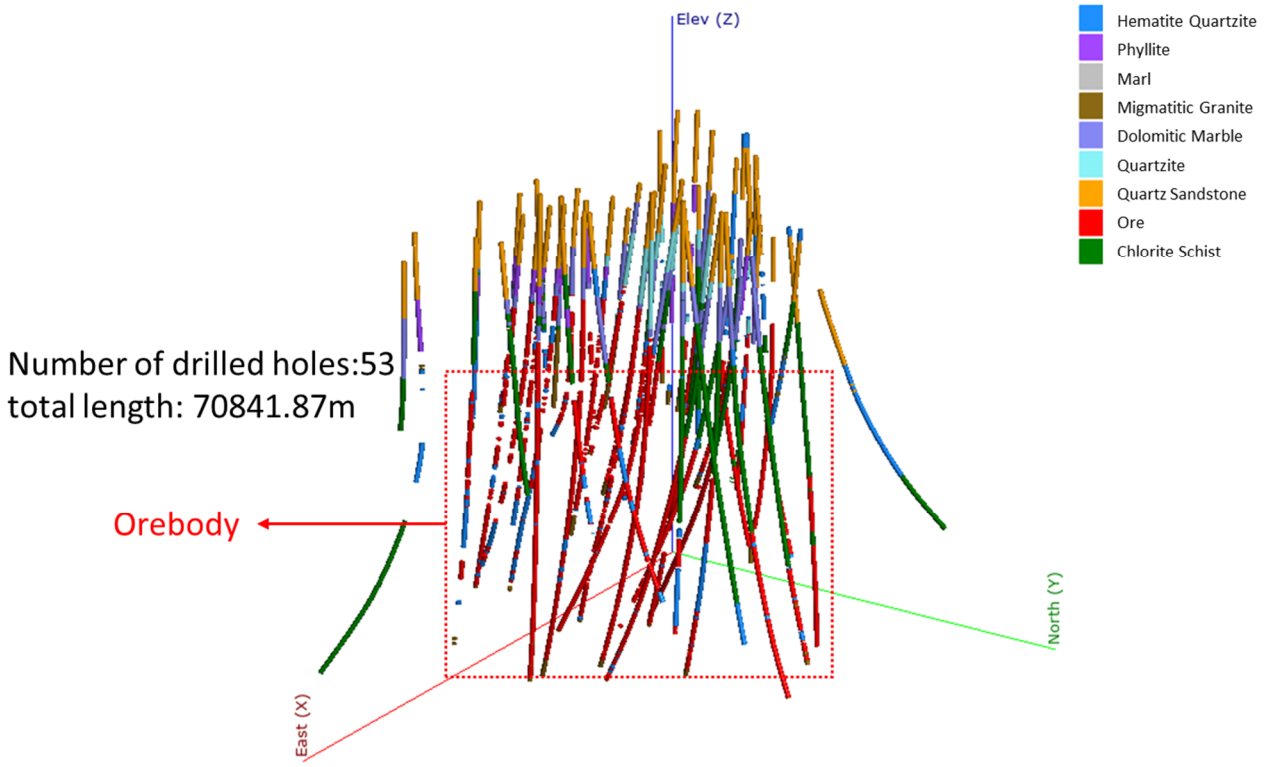

Figure 2 Geological drilling database

Using implicit modelling methodology and employing exploration drillhole data as the primary dataset, this study aims to enhance the technology for rapid construction of 3D geological models. The proposed methodology encompasses data preprocessing, geological model construction and block model generation as its primary components. Data organisation entails information collection, extracting modelling information and structuring it into a series of table files. The drillhole table typically consists of three sections: collar, survey and drillhole attributes. The collar section records the spatial location information of the drillholes while the survey section stores inclination data. The drillhole attribute table contains various properties, including lithology. Prior to importing the table structure into the 3D geological modelling software it is essential to ensure the data structure follows the software's specifications. The specific formatting requirements for the table structure, as prescribed by the supported table format, follow:

- collar — ID, X, Y, Z, max-depth
- survey — ID, depth, dip, azimuth
- properties — ID, from, to, property1, property2.

A total of 53 drillholes with a total length of 70,841.87 m (Table 1) have been identified within the Sishanling deposit, each providing comprehensive information including basic drillhole details and attributes. After importing the drillholes, their information can be displayed according to the specified requirements on the platform (Figures 2 and 5).

Table 1 Drillhole statistics for the Sishanling mine

Exploration lines	Hole ID							
0	ZK001	ZK002	ZK003	ZK004	ZK005	ZK006	ZK007	ZK008
1	ZK102	ZK103	ZK104	ZK105	ZK106	ZK107	ZK13	
2	ZK201	ZK202	ZK203	ZK204	ZK205	ZK206	ZK207	
3	ZK301	ZK302	ZK303	ZK304	ZK305			
5	ZK501	ZK502	ZK503	ZK504	ZK505			
6	ZK601	ZK602	ZK603	ZK606				
9	ZK901	ZK902	ZK903					
10	ZK1001							
13	ZK1301							
14	ZK1401	ZK1402	ZK1402-1	ZK1403	ZK1405			
16	ZK1601							
18	ZK1802	ZK1803	ZK1810					
20	ZK2001	ZK2002	ZK2004					

2.2 Surface modelling

A surface model of the study area was extracted and exported as a DXF format. A scatter plot depicting surface topography was subsequently generated using geological modelling software and based on this plot a surface model was constructed (Figure 3a). The model effectively visualised the undulating terrain for the mine areas. The satellite image is aligned carefully with the surface model, which gives a composite model that integrated a satellite image (Figure 3b). This method facilitated a detailed visualisation of the spatial relationship between the drillholes and surface features, thus achieving a more realistic representation. The surface model plays a pivotal role in the entire 3D geological modelling process. Establishing a surface model for the Sishanling mine accurately captures variations in surface undulations, facilitating a clear understanding of the spatial relationship between the surface mine conditions and the surroundings. In addition, the surface model assists in faithfully regenerating ground vertical stress distribution for subsequent numerical simulations.

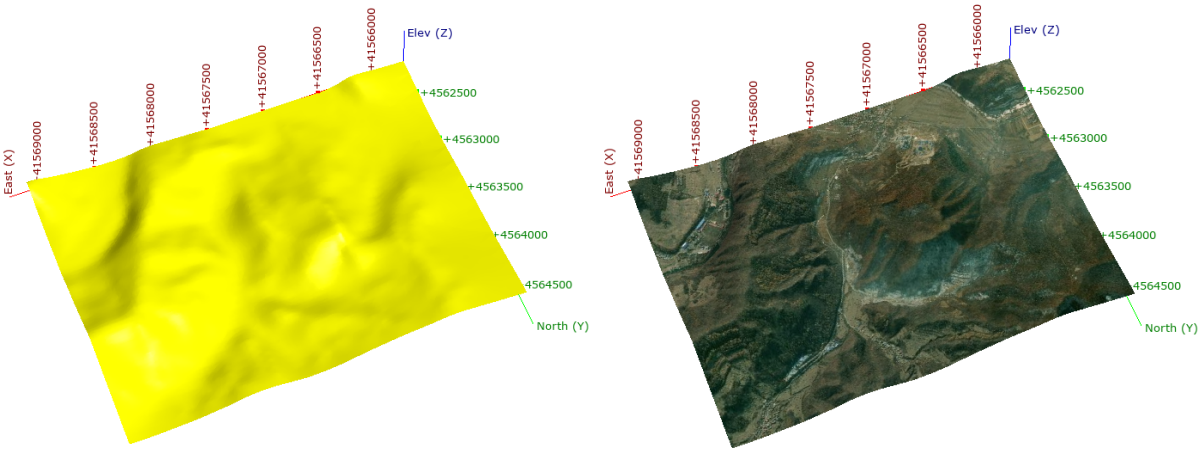

(a) (b)

Figure 3 Surface model. (a) Topography; (b) Satellite photo

2.3 Modelling scope

Reasonable modelling dimensions are required as the foundation of a precise 3D geological model. The modelling depth range was determined through statistical analysis based on existing drillholes and the exploration profile data, allowing for the statistical determination of both elevation and depth ranges in the study area (as shown in Figure 4). The location of the drillholes is illustrated in Figure 5. The maximum elevation of the surface area is 381.877 m and the depth of the drillholes is approximately 2,000 m. To sum, the Z-axis range of the model is set to 520 m to –2,400 m, and the modelling range is shown in Table 2.

Table 2 The scope of the 3D geological model

	Min (m)	Max (m)	Length (m)	Area (km²)
X (east)	41,566,300	41,569,000	2,700	6.21
Y (north)	4,562,400	4,564,700	2,300	
Z (elevation)	–2,400	520	2,920	

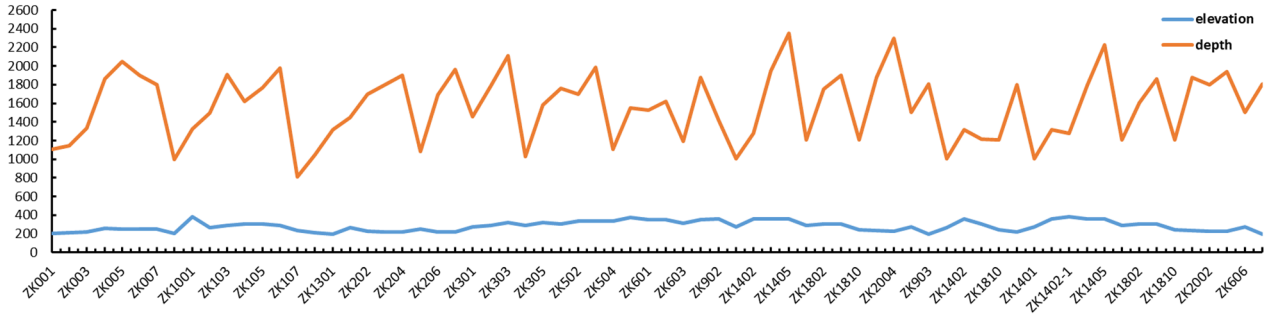

Figure 4 Basic data elevation along with different depths of exploration drill boreholes

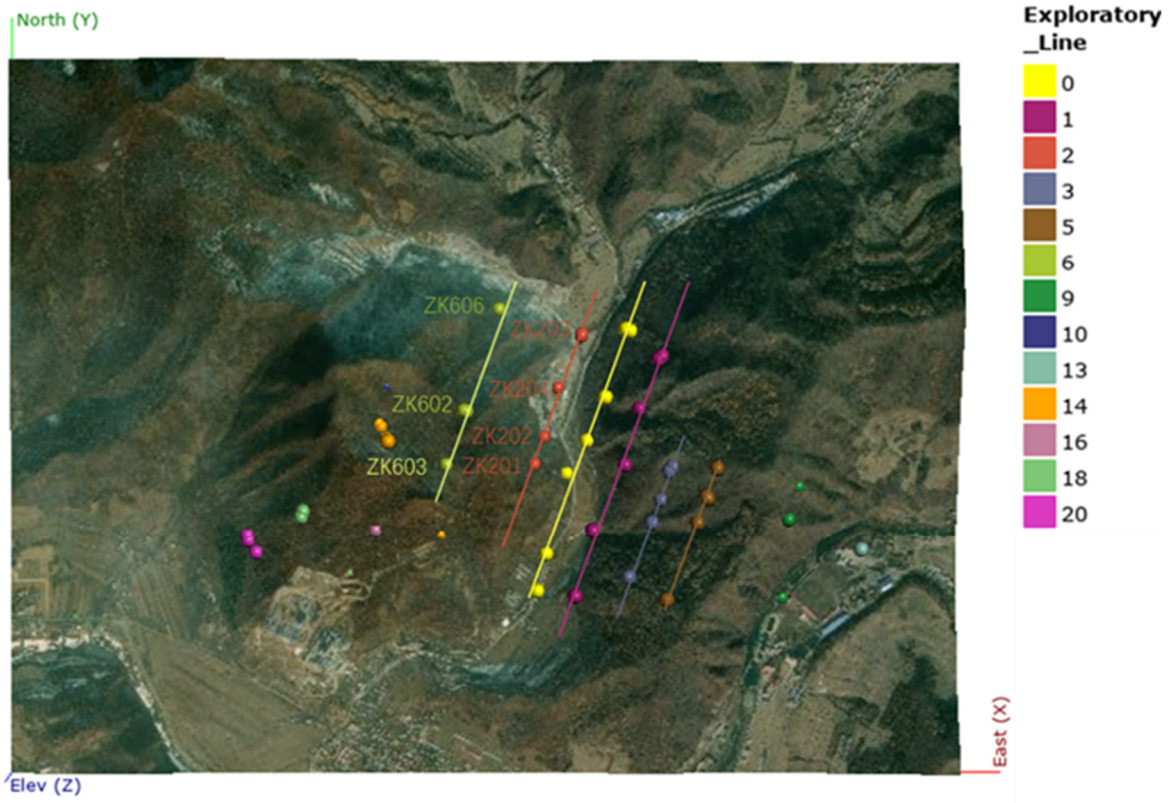

Figure 5 Exploration line and drilling location

2.4 Geological model

The stratigraphic model represents a critical element within the study area. In this work, the approach in constructing the stratigraphic model involved simplifying and categorising the lithology of the drillholes. Subsequently, stratigraphic interfaces were generated from the drillhole data sequentially, following the stratigraphic contact surface relationships. Finally, the model was validated against the exploration line section. The model was further refined by removing any erroneous control points and further refining the stratigraphic interfaces.

The lithology of the drillholes was simplified and categorised, and it was found that the Sishanling mine area contains nine major lithologies (as shown in Figure 6). According to the stratigraphic contact surface relationships, the corresponding interfaces were constructed and modified, and the interfaces are shown in Figure 6a. A subsequent generation of the geological model was conducted based on the interfaces (Figure 6b).

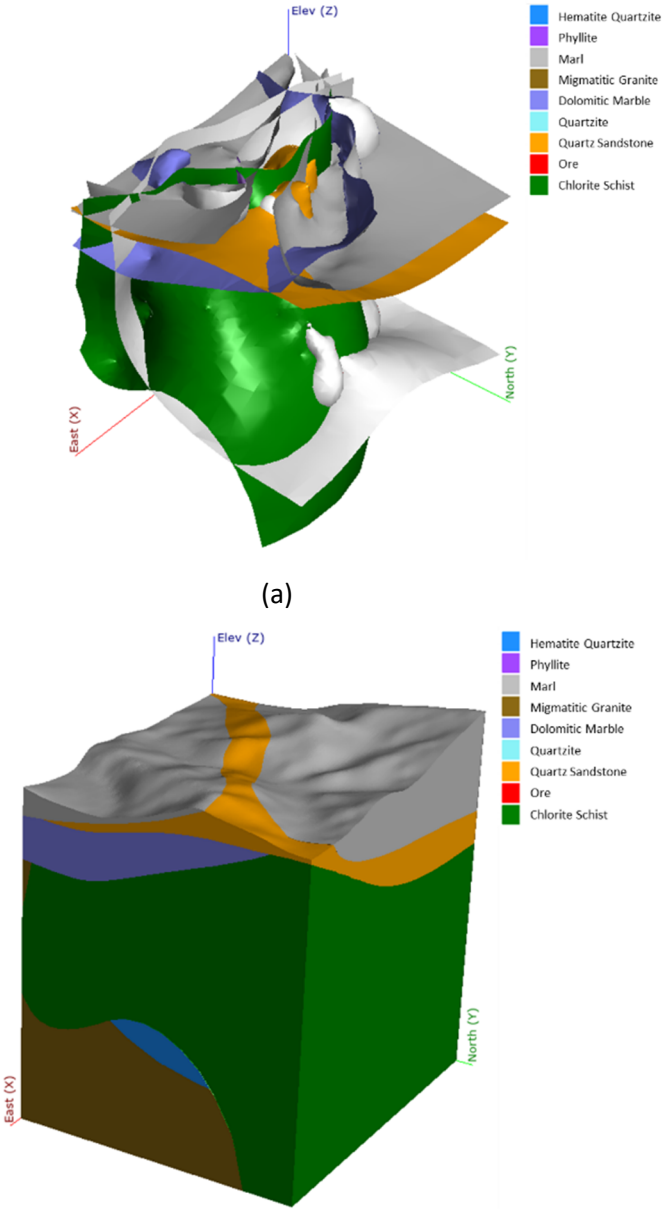

Figure 6 3D geological model generation. (a) Stratigraphic interfaces; (b) Geological model

2.5 Geological model calibration

Once the geologic model was constructed, it must have a validation process to ensure its accuracy (Jones et al. 2008), thus enhancing its efficacy in the subsequent phase of mine production design. In this study, the model was validated by back-flagging drillhole data. A new lithology table was generated based on the constructed model and then comparing it with the original drillhole lithology table to count the matches (Table 3). Model validation is conducted to confirm the correlation between the generated model and the drillhole data. Table 4 shows that the matching percentages are greater than 85% for the majority of the lithology, although two matching percentages seem to be lower for the phyllite (83.82%) and chlorite schist (79.95%). In general, the geological model generated can be considered as a good one to represent the geology of Sishanling mine.

Table 3 Drilling borehole data calibration based on the drillhole lithology matching percentage

Drilling lithology	Drilling length (m)	Matching length (m)	Matching percent (%)	Non-matching length (m)	Non-matching percent (%)
Marl	7,751.8	7,649.648	98.68%	102.152	1.32%
Quartz sandstone	11,645.04	10,617.611	91.18%	1,027.429	8.82%
Quartzite	2,790.48	2,743.641	98.32%	46.839	1.68%
Phyllite	2,834.08	2,375.554	83.82%	458.526	16.18%
Dolomitic marble	5,443.7	4,652.11	85.46%	791.66	14.54%
Chlorite schist	10,408.88	8,321.435	79.95%	2,087.445	20.05%
Orebody	22,165.17	21,830.901	98.49%	334.269	1.51%
Migmatitic granite	1,705.21	1,507.944	88.43%	197.266	11.57%
Hematite quartzite	6,097.51	5,648.734	92.64%	448.776	7.36%

2.6 Block model

The block model of Sishanling mining area facilitates the 3D visualisation of geological morphology and provides a comprehensive understanding of a deep mining environment. Initially the modelling scope and unit block size were pre-determined, with the former aligning with the geological model scope (Table 2). The selection of the unit block size significantly influences subsequent optimisation of the mining sequence. Although a smaller block size theoretically yields more precise results and enhances the representation of orebodies, aiding rock mass attribute analysis, excessively small blocks can overwhelm computational resources, resulting in slow calculation speeds. The selection of the block size heavily impacts numerical simulation outcomes. It is necessary to divide the model into different block sizes based on actual geological features and a balanced consideration of multiple factors. These factors include the extent of exploration, the geological and morphological characteristics of the orebodies, mining methods, equipment and computational power. Consequently, unit blocks in the geological model are delineated with dimensions of 20 × 20 × 20 m, resulting in a total of 2,266,500 unit blocks within the block model (Figure 7).

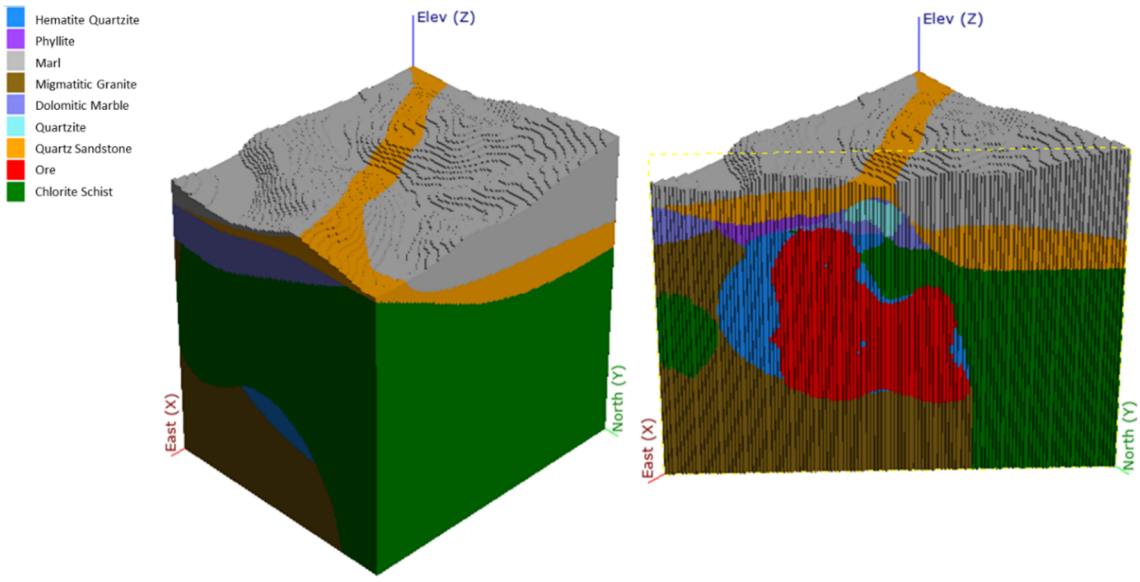

Figure 7 Block model for Sishanling iron mine

3 Large mine-scale and local region-scale geomechanical model

3.1 Geometric mine-scale model

A comprehensive dataset for mine design was acquired, including excavation structure, roadway cross-section and mid-section plan drawings for key components such as shafts, roadways, chutes, chambers and stopes within the Sishanling mine. This dataset underwent preprocessing before geometric models of the mine shafts were developed using a hybrid modelling approach. Leveraging the capabilities of GeoSlam's high-resolution scanner, specific areas requiring detailed representation underwent scanning. Meanwhile, certain underground excavations were modelled by converting 2D drawings into 3D models. Subsequently, models generated using these two methodologies were integrated to create the final comprehensive geometric model. The results of the geometric model are shown in Figure 8.

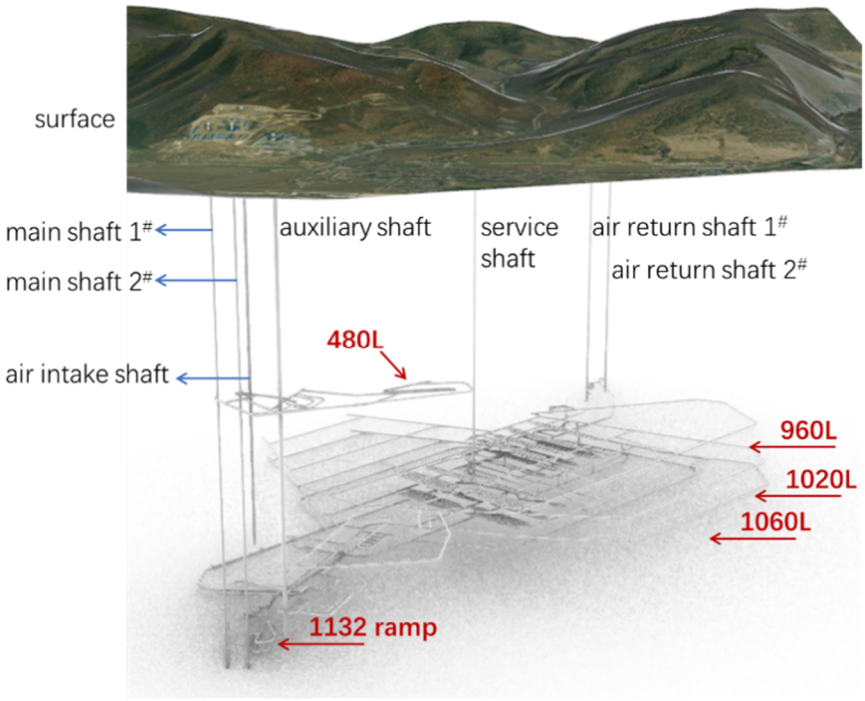

Figure 8 Geometric model of Sishanling mine

3.2 Sub-blocked local-scale model

To achieve a mixed large-scale and local refinement model, the block units needs to be subdivided based on the geometric models and modeller-specific considerations. These geometric models include shafts, ramps, chambers and levels, among others. Initially, the geometric model is imported as a 'mesh'. Subsequently, the mesh is used as the trigger condition for mesh subdivision, resulting in the subdivision of the parent block cells. According to the distance between the block units and the geometric model, the size of the edge unit length is reduced to 1.0 m so as to encompass the whole mine, allow local refinement and simplify the calculation. As a result, the total number of final block model units is 6,166,600.

3.3 Mechanical parameter interpolation

The point load test has been recognised as a practical field test for fast rock strength estimation. A point load test campaign was conducted in 53 drillholes at an interval of approximately 50.0 m. It should be mentioned that the 50.0 m interval was not fixed and it was reduced to a smaller distance (i.e. 5.0 or 10.0 m) if the rock type or condition are changed. The locations of rock point loads were identified and the number of specimens for rock point load testing was determined accordingly. The relationship between unconfined compressive strength (UCS) and the point load strength can be expressed as:

$$UCS = K \times Is_{50} \tag{1}$$

where K is the 'conversion factor' and Is_{50} is the point load strength index. A conversion factor K = 21~22 worked well for a variety of rock types and geographic regions (Rusnak & Mark 2000). Using point load data from drillholes and the point load strength index, uniaxial compressive strength and tensile strength were determined and interpolated using a cubic spline interpolation method within a depth range of 0 to 2,000 m at 10 m intervals.

All drilling mechanical parameter data were aggregated into 4,160 items, which were then organised into a CSV format and imported into the geological modelling software. A numerical model was subsequently constructed based on the data. The numerical model was interpolated and then integrated into the sub-blocked model to determine the mechanical parameters of the block model, as shown in Figure 9.

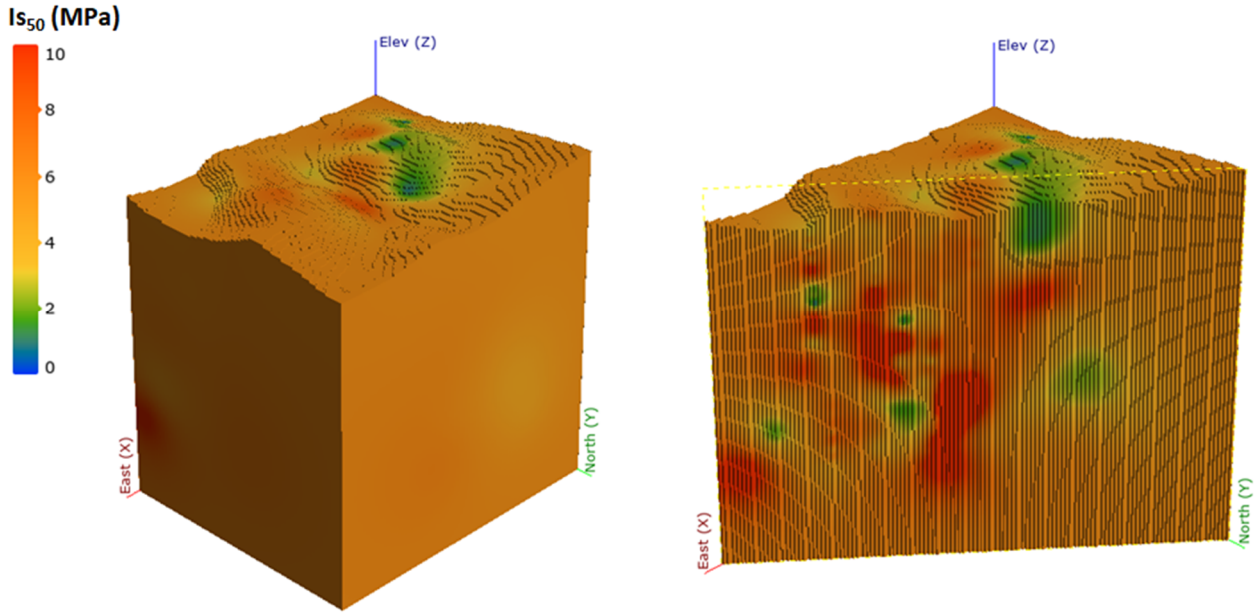

Figure 9 Is_{50} distribution of the mine-scale model

3.4 Data conversion

Due to the lack of a direct output data format between the geological modelling software and FLAC3D, it was necessary to conduct research on converting block model unit data to facilitate the importation of block models and mechanical parameters into FLAC3D. The block model was exported to a CSV file format from the geological software and the unit information of the block model is delineated, as seen in Table 4. The block units were regular hexahedrons where X, Y and Z represent the coordinates of the unit's centre of mass, and XINC, YINC, ZINC represent the unit's dimensions. The term 'litho' denotes the lithology of the unit, while the remaining parameters specify the mechanical properties of the unit.

In accordance with the FLAC3D command format, the coordinates (X, Y, Z) of nodes P0 to P3 within the hexahedral unit of FLAC3D were computed using the unit's centre of mass coordinates in Matlab. These computed coordinates, in conjunction with the unit's lithology, were employed to generate a FLAC3D pre-processing data file (.dat text file) for the creation of a model grid with the mechanical properties necessary for FLAC3D modelling.

Table 4 Sub-blocked model unit information

X	Y	Z	XINC	YINC	ZINC	Litho	Is_{50} (MPa)	UCS (MPa)	Tensile (MPa)
41,566,310	4,562,410	–2,390	20	20	20	Migmatitic granite	5.71	125.54	0.513
41,566,310	4,562,410	–890	20	20	20	Phyllite	5.72	125.87	0.515
41,566,310	4,562,410	–250	20	20	20	Quartz sandstone	6.55	144.06	0.619
41,566,310	4,562,750	–750	20	20	20	Chlorite schist	5.53	121.64	0.491
41,566,310	4,563,930	270	20	20	20	Marl	5.13	112.86	0.441

4 Numerical simulation analysis

4.1 FLAC3D modelling

The data file from Section 3.4 was imported into FLAC3D and a large mine-scale model with a refined local-scale model was built for the entire mine. The hexahedral elements of FLAC3D are in accordance with the block model units described in Section 3.2. The model dimensions, as illustrated in Figure 10, are 2,700 × 2,300 × 2,920 m. The model comprises approximately 6 million computational elements, primarily categorised into different rock groups according to the lithologies.

4.2 Constitutive models

Different lithologies were assigned distinct constitutive models in the modelling. For the rock mass a strain softening constitutive model was employed to consider the brittleness behaviour of hard rock and the strain softening behaviour of a typical rock mass. Backfilling, with a low modulus of elasticity and a relatively lower stress state compared to the surrounding rock mass, necessitates consideration of its yielding and destruction. For simplicity, the Mohr–Coulomb model was employed for the backfilling materials. The null model was used for the excavation.

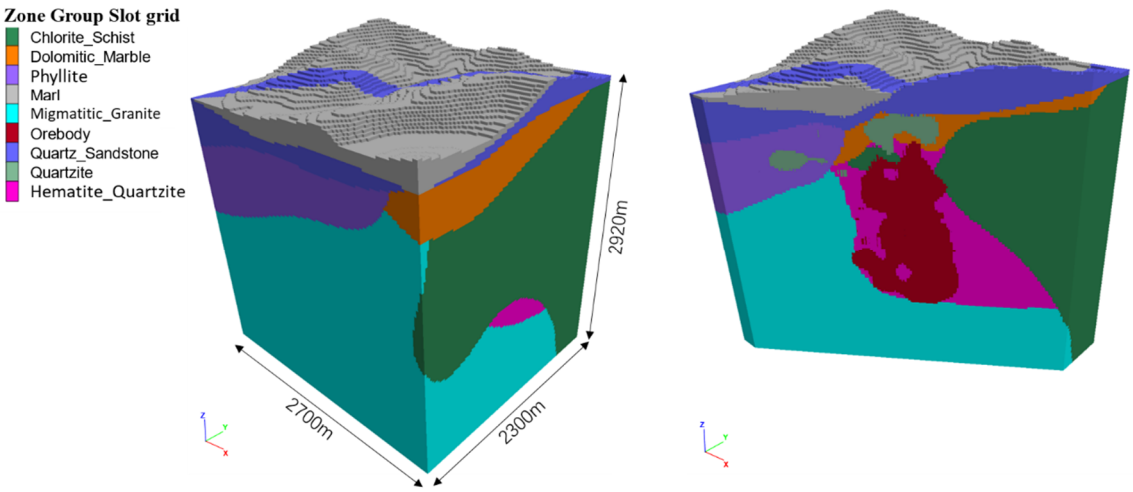

Figure 10 FLAC3D numerical model with nine rock type domains

4.3 Mechanical parameters estimation

The values of Is_{50}, UCS and tensile strength were assigned to each zone from the data file in Section 3.4 using FISH coding in FLAC3D. The elastic modulus of rock can be calculated according to the following empirical equation (He et al. 2011):

$$Ei = 350UCS \tag{2}$$

where:

Ei = elastic modulus of rock

UCS = uniaxial compressive strength.

According to the Hoek–Brown criterion (Hoek & Brown 2019), the elastic modulus of a rock mass can be calculated by the following equation:

$$E_{rm} = Ei\left(0.02 + \frac{1}{1+\exp[(60+15D-GSI)/11]}\right) \tag{3}$$

where:

E_{rm} = elastic modulus of rock mass

Ei = elastic modulus of rock

D = a factor which depends upon the degree of disturbance to which the rock mass has been subjected to by blast damage and stress relaxation

GSI = the geological strength index.

From the Mohr–Coulomb criterion, the cohesion can be calculated by the following equation:

$$C = \frac{UCS \times (1-\sin\varphi)}{2\cos\varphi} \tag{4}$$

where:

C = cohesion

UCS = uniaxial compressive strength

φ = internal friction angle.

According to the relevant empirical equations (Hudson et al. 2000), Poisson's ratio and the geological strength index have the following relation:

$$\nu = 0.32 - 0.0015GSI \tag{5}$$

where:

ν = Poisson's ratio

GSI = the geological strength index.

To consider the brittle behaviour of the strain softening model, the critical stain is assumed to be 1% for both the cohesion and friction angle, based on previous works. In addition, the residual cohesion is considered as 10% of the peak cohesion, the residual internal friction angle is 120% of the peak internal friction angle and the residual tensile strength is assumed to be 0.

For the backfilling process, the goaf was divided into the bottom (10 m), the middle and the top; each to be filled with different strengths of slurry. The bottom was filled with a 1:8 cement-sand ratio filling slurry, while the middle and top were filled with a 1:10 cement-sand ratio filling slurry. With Mohr–Coulomb applied to the backfilling, the evolution of the filler from loose to gravity-settled consolidation was simulated by first assigning a value of zero to cohesion and tensile strength, and then assigning the material values in Table 5 after the consolidation stage. The material parameters in Table 5 were derived from the measured values of the experiments.

Table 5 Physical and mechanical parameters of the simulated backfill materials

Cement-sand ratio	Density (kg/m³)	Elastic modulus (MPa)	Poisson's ratio	Compressive strength (MPa)	Cohesion (MPa)	Internal friction angle (°)	Tensile strength (MPa)
1:10	2,000	462.83	0.3	1.65	0.448	33	0.224
1:8	2,100	510.51	0.3	1.82	0.494	33	0.247

4.4 In situ stress

Based on the technical report of in situ stress measurement (Peng et al. 2012), the surface elevation of the drillhole is about 225 m and the maximum depth of the hole is less than 1,200 m. According to the report, the in situ stress can be estimated as:

$$\begin{aligned} S_H &= 0.4619 + 0.0389D \\ S_h &= 0.5245 + 0.0283D \\ S_V &= \rho g D \end{aligned} \tag{6}$$

where:

S_H = maximum horizontal principal stress

S_h = minimum horizontal principal stress

S_V = vertical stress

D = the depth of the drillhole (positive downward).

The direction of the maximum horizontal principal stresses in drillholes GK-3# and GK-8# are N52.4°, NE73.8°, NE68.5° and NE76.6°, respectively, which are close to the north-northeast, and the average direction is 67.83°. It should be mentioned that the stress orientation in the drilling holes shows certain differences that can reach up to 24.2° in a northeast direction. The in-situ stress shows certain spatial variations so to consider an

average' simple situation, the direction of maximum principal stresses in the simulation was taken as NE67.83° in the following modelling.

4.5 Modelling result and discussion

4.5.1 Excavation sequence

The designed stopes are divided into primary and secondary stopes. The primary stopes are encased completely within the orebody while the secondary stopes could face two to three sides of backfilling stopes. The stopes are strategically spaced apart to prevent interference between drilling, mining and filling operations, as well as to avoid excavating or drilling of the backfilling. After completing the initial mining step the area is filled before works advance to mining on the adjacent sides. Mining adjacent to the second mining step resumes once the filled area reaches the design strength and continues until the end of the two-step mining area is attained, after which refilling occurs. The complete excavation sequence within the panel area extends from the centre of the orebody to the flanks of the retreat excavation. This initially involves mining from the centre outwards to the designated mining zone, as indicated by arrows 1 in Figure 11, followed by retreat mining on either side of the stopes, as illustrated by arrows 2.

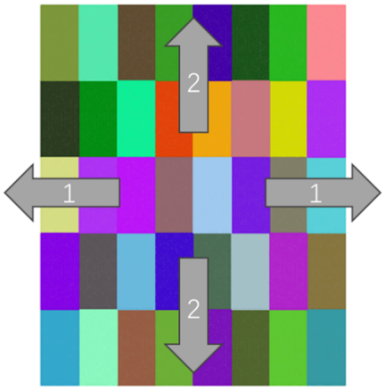

Figure 11 Horizontal section of excavation sequence in the panel area

4.5.2 Development and excavation modelling results

Figure 12 shows a contour of maximum principal stress on the horizontal plane of a –1,020 m drift. It is evident that there are virtually no areas of high stress concentration following completion of the shaft and drifts excavation. The contours of the stress field, plastic zone and displacement field on vertical planes are shown for the four stopes at the 1020 L of the first excavation (Figure 13). The contour indicates that stresses concentrated around the excavated stopes following the excavation of the four stopes in the first mining stage. This concentration is primarily observed at the arch corners of the stopes. Considering the plastic zone in conjunction with the displacement field reveals that its influence range is limited and will not significantly impact the overall stability of the stope.

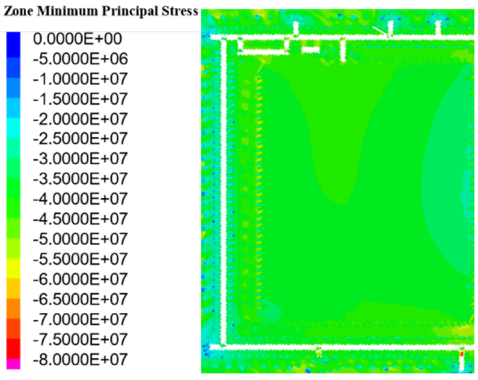

Figure 12 Contour of maximum principal stress on the horizontal plane of a –1,020 m drift

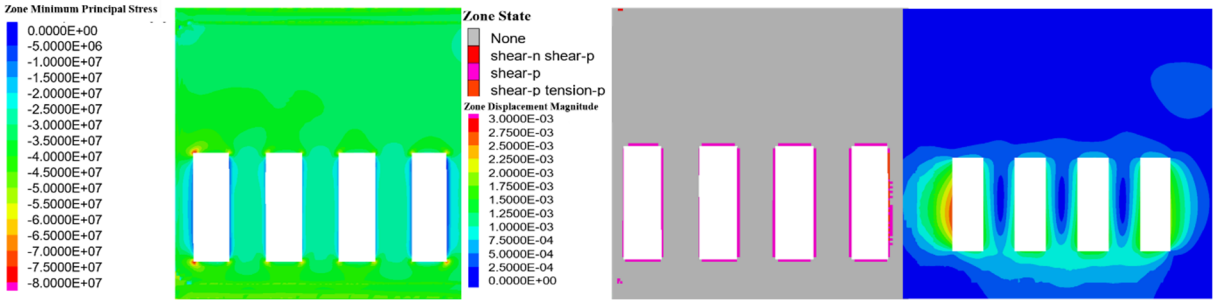

Figure 13 Contours of maximum principal stress, zone state and displacement on a vertical plane

4.5.3 Backfilling

Analysis of the three stress components (XX, YY, ZZ) in Figure 14a shows that the solidification of the filling body occurs due to the effect of self-weight. Additionally, the hydrostatic pressure at the bottom of the filling body, calculated as *pgh* (where h = 60 m), is approximately 1.5 MPa. Upon comparing the three stress components within the filling body, the distribution range appears reasonable. Furthermore, the stress distribution within the filled body remains largely uninfluenced by the in situ stress during the initial stages under self-weight. Notably the stress within the filled body is significantly lower compared to the surrounding rock mass (Figure 14b).

The excavation progresses in a pyramid-like manner, starting with mining of the central panel area of the block. It suggests that the excavation process initiates from the panel area of the lower level. Subsequently, as a space is formed within the panel area, excavation operations progress to the upper level; maintaining a larger excavation area for the lower level than the upper level. This mining sequence is conducive to effectively reducing stress concentration.

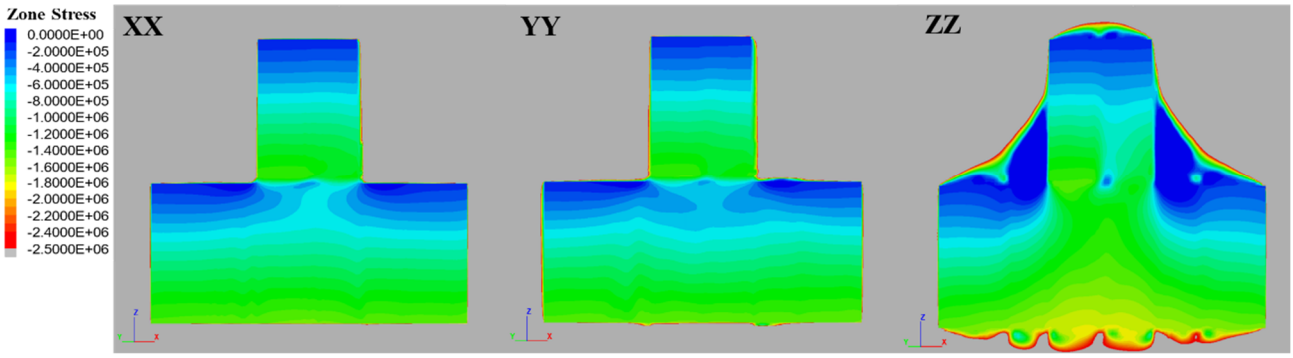

(a)

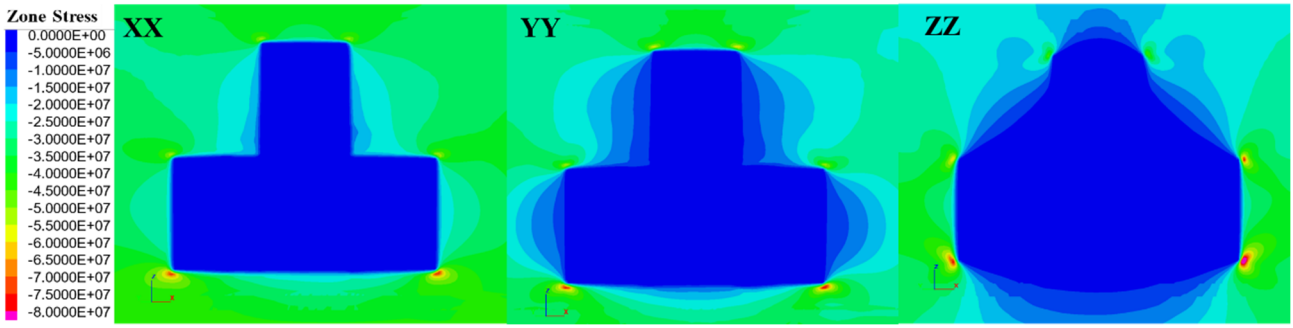

(b)

Figure 14 Stress distribution within the backfilling stope on a vertical plane: (a) Legend for 0–2.5 MPa; (b) Legend for 0–80 MPa

5 Conclusion

The construction of a 3D geological model utilised implicit modelling, with drillhole data serving as the primary geological information. The key components of the modelling approach consisted of data preprocessing, geological interfaces and block models. Furthermore, a campaign was conducted to determine the mechanical parameters for core samples from drillholes; the test results of which were then interpolated and assigned into the block elements within the geological model. Using the scanned geometry data of ramps, drifts, crosscuts and, notably, the designed stope geometry, a mine-scale numerical model built using FLAC3D software was used to assess the stability of stopes at various mining levels. A numerical simulation method was proposed to encompass the entire mining cycle, including development, mining and backfilling, and was specifically designed for underground metal mines. The evolution of stress was then analysed for the designed mining stope sequences. This study presents a practical numerical approach for underground mine-scale numerical analysis.

Acknowledgement

Benxi Longxin Mining staff members who have collected and processed critical geological, geotechnical and drillhole data are greatly appreciated.

References

He, P, Liu, CW, Wang, C, You, S, Wang, WQ & Li, L 2011, 'Correlation analysis of uniaxial compressive strength and elastic modulus of sedimentary rocks', *Journal of Sichuan University (Engineering Science Edition)*, vol. 43, no. 4, pp. 7–12.

Hoek, E & Brown, ET 2019, 'The Hoek-Brown Failure Criterion and GSI-2018 Edition', *Journal of Rock Mechanics and Geotechnical Engineering*, vol. 11, no. 8, pp. 445–463.

Hudson, JA & Harrison, JP 2000, *Engineering Rock Mechanics: an Introduction to the Principles*, Elsevier Science, Pergamo.

Jones, RR, Mccaffrey, KJ, Imber, J, Wightman, R, Smith, SA, Holdsworth, RE & Wilson, RW 2008, 'Calibration and validation of reservoir models: the importance of high resolution, quantitative outcrop analogues', *Geological Society*, vol. 39, no. 1, pp. 87–98.

Kaufmann, O & Martin, T 2009, 'Reprint of "3D geological modelling from boreholes, cross-sections and geological maps, application over former natural gas storages in coal mines" [Comput. Geosci. 34 (2008) 278–290]', *Computers & Geosciences*, vol. 35, no. 1, pp. 70–82.

Peng, H, Ma, XM, Jiang, JJ, Bai, JP 2012, *Liaoning Benxi Sishanling Iron Mine Hydraulic Fracturing Stress Measurement and Analysis Report, Sishanling Iron Mine, Benxi*, Institute of Geomechanics, Chinese Academy of Geological Sciences.

Rusnak, J & Mark, C 2000. 'Using the point load test to determine the uniaxial compressive strength of coal measure rock', *Geology*, vol. 18, no. 5, pp. 1–10.

Wang, B, Wu, L, Li, W, Qiu, Q, Xie, Z, Liu, H, & Zhou, Y 2021, 'A semi-automatic approach for generating geological profiles by integrating multi-source data', *Ore Geology Reviews*, vol. 34, no. 10, pp. 104–110.

Yu, M, Wu, J, Wang, Y, Shi, W & Wang, X 2023, '3D geological modeling and its application in underground space development', Journal of Disaster Prevention and Mitigation Engineering, vol. 43, no. 3, pp. 588–595.

Zhong, DY, Wang, LG, Lin, BI, & Jia, MT 2019, 'Implicit modeling of complex orebody with constraints of geological rules', *Transactions of Nonferrous Metals Society of China*, vol. 29, no. 11, pp. 2392–2399.